High-throughput physiological profiling of endosymbiotic dinoflagellates (Symbiodiniaceae) using flow cytometry

Colin J. Anthony*, Colin C. Lock, Bastian Bentlage†

Marine Laboratory, University of Guam, Mangilao, Guam, USA

* colin_anthonynw@outlook.com

† bentlageb@triton.uog.edu

Short title: Physiological profiling of Symbiodiniaceae via flow cytometry

Keywords: protocol, autofluorescence, photosynthesis, photopigments, chlorophyll, peridinin, antioxidants, symbiosis, coral reefs, Cnidaria

Abstract

Endosymbiotic dinoflagellates (Family Symbiodiniaceae) are directly responsible for coral survival during climate change, as the breakdown of the coral-dinoflagellate symbiosis leads to coral bleaching and often mortality. Despite methodological progress, assessing the physiology of Symbiodiniaceae *in hospite* remains a complex task. Bio-optics, biochemistry, or "-omics" techniques are expensive, often inaccessible to investigators, or lack the resolution required to understand single-cell physiological states within endosymbiotic dinoflagellate assemblages. To help address this issue, we developed a protocol that generates a physiological profile of Symbiodiniaceae cells while simultaneously determining cell densities using an entry-level benchtop flow cytometer. Two excitation/emission profiles in the red spectrum target light harvesting complex (LHC)-associated pigments, while green and yellow autofluorescence provides insight into antioxidant-associated pigments. Excitation/emission profiles are generated for each individual cell, simultaneously profiling thousands of Symbiodiniaceae cells, thus increasing statistical power to discriminate between groups even when effect sizes are small. As flow cytometry is adopted as a robust and efficient method for endosymbiont cell counting, integration and expansion of our protocol into existing workflows allows quantification of endosymbiont photophysiology and stress-signatures with minimal additional effort.

Introduction

Symbiodiniaceae are dinoflagellates known for their endosymbiotic relationship with many marine invertebrates, most notably reef building corals (LaJeunesse et al., 2018). The breakdown of this symbiosis can lead to coral bleaching and mortality (Hoegh-Guldberg 1999). Despite methodological progress identifying functional and genetic variation in Symbiodiniaceae, assessing trait variation of Symbiodiniaceae *in hospite* remains a complex task (Davies et al., 2022). Pulse Amplitude Modulated (PAM) fluorometry is widely used to quantify photosynthetic efficiency of Symbiodiniaceae photosystems *in hospite* (Warner et al. 1996) both *in situ* (e.g. Suwa et al. 2008) and *ex situ* (e.g. Berg et al. 2021). However, PAM fluorometry provides an aggregate measure of photosystem performance for the Symbiodiniaceae population and does not quantify variation in photosystem performance between cells within the symbiont population. Isolation, characterization, and quantification of photopigments is laborious and time consuming, relying on the extraction of pigments from cells prior to analysis, followed by the normalization of measured pigment quantities to observed cell densities or overall protein content (e.g. Hennige et al. 2009; Fernandes de Barros Marongoni et al. 2020).

By contrast, flow cytometry has been used to quantify photophysiologcal parameters from both plankton (Dubelaar and Jonker 2000) and cnidarian-associated Symbiodiniaceae (Lee et al. 2012), is commonly used for determining endosymbiont cell densities (Krediet et al. 2015), and requires comparatively little sample preparation. However, Symbiodiniaceae photosystem composition differs from other photoautotrophs, a fact that needs to be considered during data interpretation. Additionally, the impact of batch effects and sample degradation has not been well-studied for applications that employ flow cytometry for physiological profiling of Symbiodiniaceae. To address these issues and provide guidelines for simultaneously quantifying

Symbiodiniaceae cell densities and physiological profiles, we developed an efficient and consistent flow cytometry protocol that can be directly integrated into commonly used workflows. Our protocol generates profiles from individual cells using the high-throughput capabilities of flow cytometers, thus generating large sample sizes across multiple parameters. This protocol may be used to identify functional differences in Symbiodiniaceae assemblages between host species, sampling sites and timepoints, and potentially niche partitioning of Symbiodiniaceae populations within a single host.

Materials and Methods

Protocol

The protocol described in this article was developed using the Guava easyCyte 6HT-2L (Luminex Corporation, Austin, TX) benchtop flow cytometer and is available through protocols.io, (https://dx.doi.org/10.17504/protocols.io.dm6gpjr2jgzp/v1) and included as File S1 of this article for printing.

Symbiodiniaceae autofluorescence

Our flow cytometry protocol relies on two excitation lasers (blue and red) and emission detectors in the green, yellow, and red spectra. Excitation-emission profiles used are as follows: (1) red fluorescence (695/50 nm) off the blue (488 nm) excitation laser (RED-B), (2) red fluorescence (661/15 nm) off of the red (642 nm) excitation laser (RED-R), (3) green fluorescence (525/30 nm) and (4) yellow fluorescence (583/26 nm) off the blue (488 nm) excitation laser (GRN-B and YEL-B respectively).

Symbiodiniaceae autofluorescent signatures are dominated by photosynthetic pigments such as chlorophylls and carotenoids. Autofluorescent pigments previously identified from Symbiodiniaceae include beta-carotene, chlorophylls *a* and c_2, diadinoxanthin, diatoxanthin, and peridinin (Venn et al. 2006; Hennige et al. 2009). We also identified flavin-based fluorescent proteins (FbFPs) as a probable source of autofluorescence (Koziol et al. 2007; Mukherjee et al. 2013). To identify our autofluorescent targets, spectral properties of chl *a* and riboflavin (FbFPs), compensated for blue (488 nm) and red (642 nm) laser excitation were visualized using FluoroFinder Spectra Viewer (https://app.fluorofinder.com/ffsv/svs/). Peridinin, beta-carotene (Koyama and Hashimoto 1993), diadinoxanthin (Kagatani et al. 2022) and chl c_2 (Zapata et al. 2001; Yacobi 2012) spectra were mapped to each other using the FluoroFinder spectra and absorbance spectra from Bricaud et al. (2004).

Optimization assays

Two assays were performed to provide a framework for optimizing the protocol presented here. We also explored the integrity of fluorescent pigments when exposed to variations in light and temperature to provide guidelines for sample processing.

(1) Assay one was used to determine the impacts of time, temperature, and light conditions on samples and the resulting data. A single staghorn coral (*Acropora pulchra*) fragment was airbrushed with filtered, sterile seawater to create a 30 mL tissue slurry. The slurry was homogenized by vortexing and needle shearing, then equally distributed across four 50 mL falcon tubes. 1 mL was aliquoted from each falcon tube and immediately processed using our cytometry protocol (File S1). After aliquots were removed, falcon tubes were separated and exposed to one of four conditions: (1) dark on ice, (2) dark at room temperature (RT = 22°C), (3)

ambient light on ice, and (4) ambient light at RT. A 1 mL sample from each falcon tube was processed approximately every two hours for a total of eight hours; a final set of samples was processed after being stored in their respective conditions overnight. This yielded six samples taken at 43, 136, 236, 344, 470, and 1459 minutes after removing tissue from the skeleton. For flow cytometry, three across-well and two within-well replicates were used for data collection.

(2) Assay two was used to optimize tissue slurry dilutions and to identify possible effects of flow cytometer run times. We prepared six 1 mL tissue slurries from a single *Acropora pulchra* fragment for flow cytometry using our protocol (File S1). Before loading samples into a 96-well microwell plate, all processed tissue slurries were combined into a single 50 mL falcon tube, needle sheared, and vortexed to homogenize samples to avoid possible batch effects. 50x, 20x, 10x, 5x, 2x, and 1x dilutions of the combined tissue slurry were prepared directly in the 200 uL wells. We created a total of 16 dilution series replicates, filling all 96 wells of the plate. Each replicate dilution (2 technical replicates) was processed at ~5 min intervals until the run was complete.

Empirical application

To test our protocol empirically, three groups of clonal, tank-acclimated upside-down jellyfish medusae (*Cassiopea* sp.) were placed into three different conditions for three weeks. Group 1 (n=4) was placed in low-light conditions (50% shade), group 2 in high-light conditions (no shade) (n=4), and group 3 experienced variable environmental conditions (n=5) rotating from high-light to low-light to high-light (one week per condition). At the end of three weeks, digitate ciri (clusters of tentacle-like structures attached to the top of each oral arm) were sampled with

sterile scissors from each individual and placed in 1 mL of filtered seawater and Symbiodiniaceae cells extracted and processed following our flow cytometry protocol (File S1).

To test for differences in means across experimental groups, non-parametric Kruskal-Wallis tests (X^2) followed by post-hoc pairwise Dunn tests (Z) were performed using the FSA R package v0.9.3 (Ogle et al. 2022). All data processing and analysis was completed with R v4.1.2 (R Core Team 2021) in RStudio v1.3.1073 (RStudio Team 2020). Figures were generated and modified with a combination of ggplot2 v3.3.5 (Wickham 2016), ggpubr v0.4.0 (Kassambara 2020), and InkScape v1.1 (https://inkscape.org).

Results

Autofluorescent pigment identification

Red light emission caused by excitation with a blue laser (RED-B) represents the core light harvesting complex (LHC) pigment peridinin (Supasri et al., 2021; Kawalska et al., 2013; Jiang et al., 2012; Bujak et al., 2009) (Fig 1A). Red light emission caused by excitation with the red laser (RED-R) represents a combined emission/excitation signature of chlorophyll *a* and chlorophyll c_2 (chl *a* & chl c_2) (Niedzwiedzki et al., 2014; Scheer, 2006) despite the suboptimal excitation wavelength (642 nm) (Fig 1B).

Fig 1 Excitation/emission spectra employed by the flow cytometry protocol presented in this contribution. Excitation laser wavelengths are indicated by arrows. Lines depict absorption spectra, while lines with shaded areas illustrate compensated emission wavelengths based on the corresponding excitation laser. **A**) The blue laser (488 nm) simultaneously excited FbFPs,

diadinoxanthin, beta-carotene, and peridinin, but emission filters helped identify different pigments (**grey boxes**) **B**) The red laser (642 nm) excited chl *a* and chl c_2 with a bias towards chl c_2.

Increased green fluorescence in dinoflagellates under stress has been attributed to beta-carotene (Lee et al., 2012; Kleinegris et al., 2010). However, diadinoxanthin, diatoxanthin (Kagatani et al. 2022; Frank et al. 1996), and flavin-based fluorescent proteins (FbFPs) (Mukherjee et al. 2013; Koziol et al. 2007; Fujita et al. 2005) also emit green fluorescent light when excited by blue light (Fig 1A). Therefore, we inferred that both GRN-B and YEL-B represents the combined signature of beta-carotene, xanthophylls (diadinoxanthin and diatoxanthin), and flavins (Fig 1A).

Effects of sample preparation on degradation

Samples stored on ice and processed within approximately two hours (136 minutes) showed the most consistent signatures across all measurements (Fig 2). RED-B and RED-R autofluorescence degraded relatively quickly at ambient temperatures, but light exposure alone does not appear to have a strong effect (Figs 2A-B). GRN-B remained stable during the first two hours, regardless of treatment, but variability increased after longer incubation (Fig 2C). Interestingly, cell concentrations were more stable under ambient temperatures, but still produced consistent results when processed within 136 minutes after being stored on ice (Fig 2D).

Fig 2 Samples prepared under different light (dark vs ambient light) and temperature (on ice vs no ice) conditions produced different parameter estimates. Only samples processed on ice within roughly two hours (136 minutes) of airbrushing yielded consistent results (**dashed boxes**). RED-B (**A**) and RED-R (**B**) autofluorescence degraded quickly, but GRN-B (**C**) remained relatively

stable over time. Interestingly, cell concentrations (**D**) were more stable under ambient conditions (no ice) but produced relatively consistent results when processed within 136 minutes after being stored on ice.

Effects of dilution and flow cytometer run-time on degradation

Six dilutions (50x, 20x, 10x, 5x, 2x, and 1x) were tested 16 times each across a 96-well plate resulting in individual sample measurements of ~150,000 cells/mL for each replicate (Fig 3). The flow cytometer run took around six hours to complete. Ten-fold and five-fold dilutions in the first four rows of the 96-well plate were the most consistent. More diluted samples produced unstable means of measured parameters, while less diluted samples exacerbated degradation. RED-B fluorescence degraded with time (Fig 3A), while RED-R, GRN-B, and YEL-B fluorescence increased with time (Fig 3B-D). Cell size (forward scatter) did not show any effects of degradation, but highly concentrated samples over estimated size, likely due to cell clumping (Fig 3E). Cell roughness (side scatter) is the most stable metric suggesting low rates of cell lysis, though increasing quartile ranges in the one-fold and two-fold dilutions suggest increased susceptibility to lysis in higher concentrations (Fig 3F). Estimates of cell concentrations were heavily affected by dilution and run-time (Fig 3G).

Fig 3 Six dilutions (50x, 20x, 10x, 5x, 2x, and 1x) were tested 16 times each across a 96-well plate. The cytometry run took ~6 hours estimating ~20 minutes between each of the 16 replicates (**Time**). Ten-fold and five-fold dilutions were the most consistent for half of the plate (**dashed boxes**) suggesting that runs should be limited to ≤ 48 wells (half of a standard 96-well plate). Over- or under-dilution of samples had a large effect on resulting parameter estimates. **A**) RED-B (peridinin) fluorescence degraded over time and had more variation with 50x and 20x

184 dilutions. **B-D**) RED-R, GRN-B, and YEL-B fluorescence increased over time, presumably due
185 to heat generated by the flow cytometer. **E**) Cell size (FSC) did not change over time, but highly
186 concentrated samples led to an over estimation of cell sizes, likely due to cell clumping. **F**) Cell
187 roughness (SSC) was the most stable parameter, suggesting low rates of cell lysis. **G**) Cell
188 concentrations were heavily affected by dilution and time spent in the flow cytometer.

189 ***Upside-down jellyfish light acclimation experiment***

190 After three weeks, *Cassiopea* medusae visibly changed color with dark-acclimated individuals
191 being dark brown and light-acclimated individuals being light tan. After identifying the
192 Symbiodiniaceae cells based on a combination of forward, side scatter, and red autofluorescence
193 (RED-B) (Krediet et al. 2015), noise was removed from the dataset (RED-B-HLog < 3.04001),
194 yielding 16,134, 18,464, and 19,821 single-cell fluorescent profiles from Symbiodiniaceae of
195 *Cassiopea* from the dark, light, and variable treatment groups, respectively. Treatment
196 influenced fluorescent means for all excitation/emission parameters: RED-B ($X^2 = 386.96$, $p <$
197 0.001), RED-R ($X^2 = 316.25$, $p < 0.001$), and GRN-B ($X^2 = 535.50$, $p < 0.001$). All post-hoc
198 pairwise comparisons demonstrated a difference in means ($p < 0.01$). The only comparison with
199 an adjusted p-value > 0.001 was the dark vs variable RED-B comparison ($p = 0.002$). Light-
200 acclimated individuals had the lowest peridinin (RED-B) and chl *a* & c_2 (RED-R) signals, while
201 dark-acclimated individuals had the lowest green emission signal ('antioxidant' pigments) (Fig
202 4).

203 **Fig 4** Digitate cirri from the upside-down jellyfish, *Cassiopea* sp., were sampled and processed
204 with our flow cytometry protocol (S1 File) after three weeks of exposure to different light
205 conditions. Each pairwise comparison indicated statistically significant differences in means ($p <$

206 0.01); the most distinct distribution ($p < 0.001$) is indicated by "***". Each distribution
207 represents 16,000 - 20,000 observations, which allowed for discriminating between treatments,
208 even with small effect size. **A**) Light-acclimated individuals had the least red fluorescence off of
209 the blue laser (peridinin). **B**) Light-acclimated individuals also had the lowest red fluorescence
210 off of the red laser (chl *a* & c_2). **C**) Dark-acclimated individuals had the lowest green
211 fluorescence (antioxidants).

212

213 **Discussion**

214 ***Symbiodiniaceae pigments and autofluorescence signatures***

215 Symbiodinaceae possess two major LHC antennae, the peridinin-chlorophyll *a* protein complex
216 (PCP) and the chlorophyll *a*-chlorophyll c_2-peridinin protein complex (acpPC), which use
217 peridinin and chl c_2 as the primary light-harvesting pigments (Polívkaa et al. 2007; Hiller et al.
218 1993). A proportionate decrease in RED-B (peridinin) and RED-R (chl *a* & c_2) would indicate a
219 decrease in overall LHC abundance within the cell. Alternatively, a shift in red fluorescent ratios
220 (RED-B vs RED-R) would indicate LHC reorganization from PCP to acpPC. For example, PCP
221 complexes have been proposed to detach from the thylakoid membrane as a mode of photo-
222 acclimation (Kanazawa et al. 2014; Jiang et al. 2012; Schulte et al. 2010). Detachment from the
223 membrane and relocation of PCP would allow for the reduction of absorbed photons to protect
224 photosynthetic reaction centers during periods of environmental stress, while photoprotective
225 acpPC complexes remain bound to the thylakoid membrane during photo-acclimation. This PCP
226 mobilization should yield a shift in RED-B vs RED-R ratios given the variable pigment
227 compositions of the PCP and acpPC antennae.

Green and yellow autofluorescent signatures are representative of photo-protective and antioxidant pigments and proteins (Fig 1A). Reactive oxygen species (ROS) are a well-known byproduct of photosynthesis, which can cause cellular damage in high concentrations, especially under environmental stress (Lesser 2006). Beta-carotene is an efficient reactive oxygen species (ROS) scavenger, especially in the vicinity of high concentrations of ROS (Burton 1990; Young & Britton 1993). Diadinoxanthin and diatoxanthin are the main components in the photoprotective xanthophyll cycle, dissipating excess energy through non-photosynthetic quenching (Frank et al. 1996), alongside production of antioxidants (Smerilli et al. 2016). The most abundant FbFPs (cryptochromes and riboflavin) act as key stress regulators (D'Amico-Damião et al. 2018; Yu 2010) and induce the accumulation of antioxidants (Deng et al. 2013; Taheri and Tarighi 2010; Sandoval et al. 2008). Given the overlap in the roles of fluorescent proteins detected by GRN-B and YEL-B, we interpret green and yellow fluorescence as signatures of stress-mitigation, including excess energy dissipation through non-photosynthetic quenching and antioxidant activity.

Protocol performance and optimization

Photopigments are fragile molecules prone to degradation in ambient conditions (Schoefs 2002). Therefore, it is important to work consistently and efficiently when processing samples using the protocol presented here. Samples processed at room temperature were prone to rapid degradation, yielding imprecise estimates of fluorescent parameters compared to consistent autofluorescence-based physiological profiles for samples stored and processed on ice (Fig 2). However, autofluorescent signatures still changed dramatically after tissue removal from coral skeletons when processing was delayed, even when stored on ice. Based on our observations (Fig

2), we recommend that samples are processed for flow-cytometry within two hours of beginning sample preparation.

Cell concentration and flow-cytometer run-time are further factors to consider. Our sample had a starting concentration of ~150,000 cells/mL. Over-dilution led to variable means of parameters and high variances, while under-dilution exacerbated degradation and caused cell clumping (Fig 3). Ten- to five-fold dilutions (15,000 – 30,00 cells/mL) produced the most consistent autofluorescence signatures. Nonetheless, samples began to degrade after processing four rows (48 wells) of the 96-well plate. Therefore, we recommend loading no more than half of a 96-well plate per run with each well containing an estimated concentration of 15,000-30,000 cells/mL. The analyses presented here provide a roadmap for implementing and optimizing our flow-cytometry protocol. We recommend investing protocol optimization time upfront. Once established, our protocol should work across a diverse set of cnidarian hosts including corals, jellyfish, and hydroids, requiring little ongoing maintenance or cost.

Applications and expansion

Under different light conditions, dinoflagellates adjust their photosystems, for example, increasing LHC pigments (peridinin, chl *a*, chl c_2) in dark conditions and increasing antioxidants (diadinoxanthin) in light conditions (Johnsen et al. 1994). This response was successfully detected in *Cassiopea*-associated Symbiodiniaceae using our flow cytometry protocol. Dark-acclimated individuals displayed the highest peridinin and chl *a* & c_2 autofluorescence, while light-acclimated individuals displayed the lowest photopigment-associated autofluorescence (Fig 4A-B). Green autofluorescence displayed the inverse pattern, where dark acclimated individuals possessed the faintest green-fluorescent signatures (antioxidants) (Fig 4C). The combination of

low LHC-associated photopigment autofluorescence and elevated antioxidant fluorescence in the light-acclimated group is likely indicative of stress, while high photopigment autofluorescence in conjunction with elevated antioxidant autofluorescence in variable-condition individuals suggests active stress-mitigation and acclimation (Fig 4). Dark-acclimated individuals with low antioxidant and high photopigment autofluorescence likely represent low stress-levels and successful acclimation (Fig 4). This acclimation experiment represents an example and empirical proof of concept for the application of our protocol for relatively simple comparisons of Symbiodiniaceae assemblages originating from different host individuals.

The ability to export fluorescent profiles for every observed Symbiodniaceae cell has massive potential. As the interest in Symbiodiniaceae moves from characterization of biodiversity through the identification of clades via DNA metabarcoding to functional characterization and identification of differences in resilience, flow cytometry has the potential to reveal functional diversity of Symbiodiniaceae *in hospite*. For example, Symbiodiniaceae assemblages hosted in corals may harbor homogeneous Symbiodiniaceae assemblages with low phylogenetic diversity (one dominant genus, species, or strain) or diverse assemblages with high phylogenetic diversity (several codominant genera, species, or strains) (Davies et al. 2022). If a coral hosts a highly diverse Symbiodiniaceae assemblage, but only a single autofluorescent profile is detected using our flow cytometry protocol, one may assume functional redundancy of symbiont clades or mediation of symbiont physiology by the coral host (Fig. 5). Alternatively, if a coral hosts a low diversity Symbiodiniaceae assemblage, but multiple distinct autofluorescent profiles are detected, one may assume functional plasticity of the assemblage (Fig 5). We suggest that exploration of these concepts using flow cytometry has the potential for high-throughput characterization of Symbiodiniaceae functional diversity *in hospite*.

295 **Fig 5**: Phylogenetic diversity of Symbiodiniaceae assemblages *in-hospite* may indicate low
296 complexity (one dominant clade) or high complexity (more than one dominant clade)
297 communities (Davies et al. 2022). Autofluorescent profiles may be either convergent or
298 divergent, as shown here by PCAs of consisting of chlorophylls (**Chl**), peridinin (**Per**), and
299 antioxidants (**AO**). The combination of phylogenetic diversity and physiological profiles has the
300 potential to allow for the classification of Symbiodiniaceae assemblage functional strategies into
301 homogenous, plastic, redundant, or diverse categories. Simulated datasets were generated and
302 analyzed using R.

303 The protocol presented here targets key LHC pigments and a combination of proteins
304 known for their role in photo-acclimation and stress mitigation. Given the diverse set of
305 autofluorescent targets and available laser/filter combinations for the detection of
306 excitation/emission spectra, this protocol may be further expanded, establishing flow cytometry
307 as a cost-effective and robust technique for profiling Symbiodiniaceae physiology. For example,
308 the implementation of filters that separate chl *a* & c_2 would permit more intimate insight into
309 LHC rearrangements during photoacclimation. Other laser/filter combinations may also facilitate
310 physiological profiling of photo-autotrophs with alternative LHC pigments, such as fucoxanthin-
311 containing dinoflagellates (Jeffrey 1989; Yoon et al. 2002) or phycoerythrin-containing marine
312 cyanobacteria (Siddiqui and Carpenter 1992; Subramaniam and Carpenter 1999).

313

314 **Acknowledgements**

315 We would like to thank Rebecca Salas for running the upside-down jellyfish acclimation
316 experiment. We would also like to thank MacKenzie Heagy for illustrating the coral-
317 dinoflagellate assemblages shown in Fig 5. Guam NSF EPSCoR directly supported this work

through the National Science Foundation award OIA-1946352. Any opinions, findings, conclusions, or recommendations expressed in this contribution are those of the authors and do not necessarily reflect the views of the National Science Foundation.

Conflict of Interest

The authors declare no conflict of interest.

Supporting Information

S1 File. Protocol to quantify photophysiology of endosymbiotic dinoflagellates using the Guava Flow Cytometer. Also available on protocols.io: https://dx.doi.org/10.17504/protocols.io.dm6gpjr2jgzp/v1

Author Contributions

Conceptualization: Colin J Anthony, Colin C Lock, Bastian Bentlage

Data Curation: Colin J Anthony

Formal Analysis: Colin J Anthony

Funding Acquisition: Bastian Bentlage

Investigation: Colin J Anthony, Colin C Lock

Methodology: Colin J Anthony, Colin C Lock

Project Administration: Colin J Anthony, Bastian Bentlage

338 **Resources:** Colin C Lock, Bastian Bentlage

339 **Software:** Colin J Anthony

340 **Supervision:** Bastian Bentlage, Colin C Lock

341 **Validation:** Colin J Anthony, Colin C Lock, Bastian Bentlage

342 **Visualization:** Colin J Anthony

343 **Writing – Original Draft Preparation:** Colin J Anthony

344 **Writing – Review & Editing**: Bastian Bentlage, Colin J Anthony, Colin C Lock

345

References

Berg JT, David CM, Gabriel MM, Bentlage B. Fluorescence signatures of persistent photosystem damage in the staghorn coral *Acropora* cf. *pulchra* (Anthozoa: Scleractinia) during bleaching and recovery, Mar. Biol. Res. 2021; 16(8-9):643-655. https://doi.org/10.1080/17451000.2021.1875245

Bricaud A, Claustre H, Ras J Oubelkheir K. Natural variability of phytoplanktonic absorption in oceanic waters: Influence of the size structure of algal populations. J. Geophysical Research Oceans. 2004; 109(C11). https://doi.org/10.1029/2004JC002419.

Bujak Ł, Piatkowski D, Mackowski S, Wörmkeb S, Jungb C, Bräuchleb C, Agarwalc A, Kotovc NA, Schulted T, Hofmannd E, Brotosudarmoe THP, Scheere H, Govorovf AO, Hilleret RG. Plasmon enhancement of fluorescence in single light-harvesting complexes from *Amphidinium carterae.* Acta Phys. Pol. 2009; 116:S22-S25. https://doi.org/10.12693/APhysPolA.116.S-22

Burton GW. Antioxidant properties of carotenoids. J. Nutr. 1990; 119:109–111.

Davies S, Gamache MH, Howe-Kerr LI, Kriefall NG, Baker AC, Banaszak AT, Bay LK, Bellantuono AJ, Bhattacharya DC, Debashish C, et al. Building consensus around the assessment and interpretation of Symbiodiniaceae diversity. 2022. https://doi.org/10.20944/preprints202206.0284.v1

D'Amico-Damião V, Carvalho RF. Cryptochrome-related abiotic stress responses in plants. Front. Plant Sci. 2018; 19. https://doi.org/10.3389/fpls.2018.01897

366 Deng B, Jin X, Yang Y, Lin Z, Zhang Y. The regulatory role of riboflavin in the drought
367 tolerance of tobacco plants depends on ROS production. Plant Growth Regul. 2014;
368 72:269–277. https://doi.org/10.1007/s10725-013-9858-8

369 Dubelaar GB, Jonker RR. Flow cytometry as a tool for the study of phytoplankton. Scientia
370 Marina. 2000; 64(2):135-136. https://doi.org/10.3989/scimar.2000.64n2135

371 Fernandes de Barros Marangoni L, Ferrier-Pagès C, Rottier C Bianchini A, Grover R.
372 Unravelling the different causes of nitrate and ammonium effects on coral bleaching. Sci.
373 Rep. 2020; 10:11975. https://doi.org/10.1038/s41598-020-68916-0

374 Frank, Cua A, Chynwat V, Young A, Gosztola D, Wasielewski MR. The lifetimes and energies
375 of the first excited singlet states of diadinoxanthin and diatoxanthin: the role of these
376 molecules in excess energy dissipation in algae. Biochim. Biophys. Acta Bioenerg. 1996;
377 1277:243-252.

378 Fujita S, Iseki M, Yoshikawa S, Makino Y, Watanabe M, Motomura T, Kawai H, Murakami A.
379 Identification and characterization of a fluorescent flagellar protein from the brown alga
380 *Scytosiphon lomentaria* (Scytosiphonales, Pheophyceae): a flavoprotein homologous to
381 Old Yellow enzyme. Eur. J. Phycol. 2005; 40:159-167.
382 https://doi.org/10.1080/09670260500063193

383 Hennige SJ, Suggett DJ, Warner ME, McDougall KE, Smith DJ. Photobiology of *Symbiodinium*
384 revisited: Bio-physical and bio-optical signatures. Coral Reefs. 2009; 28:179-195.
385 https://doi.org/10.1007/s00338-008-0444-x

386 Hiller RG, Wrench PM, Gooley AP, Shoebridge G, Breton J. The major intrinsic light-
387 harvesting protein of Amphidinium: Characterization and relation to other light-

harvesting proteins. Photochem. Photobiol. 1993; 57(1):125–131. https://doi.org/10.1111/j.1751-1097.1993.tb02267.x

Hoegh-Guldberg O. Climate change, coral bleaching and the future of the world's coral reefs. Mar. Freshw. Res. 1999; 50:839-866.

Jeffrey SW. Chlorophyll c pigments and their distribution in the chromophyte algae. In: Green JC, Leadbeater BSC, Diver WL. (eds) The Chromophyte Algae: Problems and Perspective. Systematics Association. Clarendon, Oxford. 1989; 38:13–36.

Jiang J, Zhang H, Kang Y, Bina D, Lo CS, Blakeship RE. Characterization of the peridinin–chlorophyll *a*-protein complex in the dinoflagellate *Symbiodinium*. Biochim. Biophys. Acta Bioenerg. 2012; 1817(7):983-989. https://doi.org/10.1016/j.bbabio.2012.03.027

Johnsen G, Nelson NB, Jovine RVM, Prézelin BB. Chromoprotein- and pigment-dependent modeling of spectral light absorption in two dinoflagellates, Prorocentrum minimum and *Heterocapsa pygmaea*. Mar. Ecol. Prog. Ser. 1994; 114(3):245-258.

Kagatani K, Nagao R, Shen JR, Yamano Y, Takaichi S, Akimoto S. Excitation relaxation dynamics of carotenoids constituting the diadinoxanthin cycle. Photosynth. Res. 2022; 154:13-19. https://doi.org/10.1007/s11120-022-00944-5

Kanazawa A, Blanchard GJ, Szabó M, Ralph PJ, Kramer DM. The site of regulation of light capture in *Symbiodinium*: Does the peridinin–chlorophyll *a*–protein detach to regulate light capture? Biochim. Biophys. Acta Bioenerg. 2014; 1837(8):1227-1234. https://doi.org/10.1016/j.bbabio.2014.03.019

408 Kassambara, A. ggpubr: 'ggplot2' Based Publication Ready Plots. R package version 0.4.0. 2020.
409 https://CRAN.R-project.org/package=ggpubr

410 Kawalska D, Krajnik B, Olejnik M, Twardowska M, Czechowski N, Hofmann E, Mackowski S.
411 Metal-enhanced fluorescence of chlorophylls in light-harvesting complexes coupled to
412 silver nanowires. Sci. World J. 2013; 2013:670412 https://doi.org/10.1155/2013/670412

413 Kleinegris DMM, van ES MA, Janssen M, Brandenburg WA, Wijffels RH. (2010) Carotenoid
414 fluorescence in *Dunaliella salina*. J. Appl. Phycol. 22:645-649.
415 https://doi.org/10.1007/s10811-010-9505-y

416 Koyama Y, Hashimoto H. Spectroscopic studies of carotenoids in photosynthetic systems. In:
417 Young AJ, Britton G. (eds) Carotenoids in Photosynthesis. Springer, Dordrecht. 1993.
418 https://doi.org/10.1007/978-94-011-2124-8_9

419 Koziol B, Markowicz M, Kruk J, Plytycz B. Riboflavin as a source of autofluorescence in
420 *Eisenia fetida* coelomocytes. Photochem. Photobiol. 2007; 82(2):570-3.
421 https://doi.org/10.1562/2005-11-23-RA-738

422 Krediet CJ, DeNofrio JC, Caruso C, Burriesci MS, Cella K, Pringle JR. Rapid, Precise, and
423 Accurate Counts of *Symbiodinium* Cells Using the Guava Flow Cytometer, and a
424 Comparison to Other Methods. PLOS ONE. 2015; 10(8):e0135725.
425 https://doi.org/10.1371/journal.pone.0135725

426 Lee CS, Yeo YSW, Sin TM. Bleaching response of *Symbiodinium* (zooxanthellae):
427 Determination by flow cytometry. Cytom. Part A. 2012; 81A(10):888-895.
428 https://doi.org/10.1002/cyto.a.22111

Lesser MP. Oxidative stress in marine environments: Biochemistry and physiological ecology. Annu. Rev. Physiol. 2006; 68:253-278. https://doi.org/10.1146/annurev.physiol.68.040104.110001

Maruyama S, Shoguchi E, Satoh N, Minagawa J. Diversification of the light-harvesting complex gene family via intra- and intergenic duplications in the coral symbiotic alga *Symbiodinium*. PLOS ONE. 2015; 10:e0119406.

Mukherjee A, Walker J, Weyant KB, Schroeder CM. Characterization of Flavin-Based Fluorescent Proteins: An Emerging Class of Fluorescent Reporters. PLOS ONE. 2013; 8(5):e64753. https://doi.org/10.1371/journal.pone.0064753

Muscatine L, Porter JW. Reef corals: Mutualistic symbioses adapted to nutrient-poor environments. BioScience. 1977; 27:454-460

Muscatine L, Falkowski PG, Porter JW, Dubinsky Z. Fate of photosynthetic fixed carbon in light- and shade-adapted colonies of the symbiotic coral Stylophora pistillata. Proc. R. Soc. Lond. B. 1984; 222:181–202.

Niedzwiedzki DM, Jiang Jing CSL, Blankenship RE. Spectroscopic properties of the Chlorophyll *a*–Chlorophyll c_2–Peridinin-Protein-Complex (acpPC) from the coral symbiotic dinoflagellate *Symbiodinium*. Photosynth. Res. 2014; 120:125-139. https://doi.org/10.1007/s11120-013-9794-5

Ogle DH, JC Doll, Wheeler P. Dinno A. FSA: Fisheries Stock Analysis. R package version 0.9.3. 2022. https://github.com/fishR-Core-Team/FSA

449 Polivka T, Hiller RG, Frank HA. Spectroscopy of the peridinin–chlorophyll-*a* protein: insight
450 into light-harvesting strategy of marine algae. Arch Biochem. Biophys. 2007; 458: 111–
451 120. https://doi.org/10.1016/j.abb.2006.10.006

452 R Core Team. R: A language and environment for statistical computing. R Foundation for
453 Statistical Computing, Vienna, Austria. 2021. https://www.R-project.org/

454 RStudio Team. RStudio: Integrated Development for R. RStudio, PBC, Boston, MA. 2020.
455 http://www.rstudio.com/

456 Sandoval FJ, Zhang Y, Roje S. Flavin nucleotide metabolism in plants. J. Biol. Chem. 2008;
457 283(45):30890-30900. https://doi.org/10.1074/jbc.M803416200

458 Schoefs B. Chlorophyll and carotenoid analysis in food products. Properties of the pigments and
459 methods of analysis. Trends Food Sci. Technol. 2002; 13(11):361-371.
460 https://doi.org/10.1016/S0924-2244(02)00182-6

461 Siddiqui PJA, Carpenter EJ. Ultrastructure and immunolocalization of phycobiliproteins and
462 ribulose 1,4-bisphosphate carboxylase/oxygenase in the marine cyanobacterium
463 Trichodesmium thiebautii. J. Phycol. 1992; 28: 320–327.

464 Smerilli A, Orefice I, Corato F, Olea AG, Ruban AV, Brunet C. Photoprotective and antioxidant
465 responses to light spectrum and intensity variations in the coastal diatom *Skeletonema*
466 *marinoi*. Environ. Microbiol. 2016; 19(2):611-627. https://doi.org/10.1111/1462-
467 2920.13545

468 Subramaniam A, Carpenter EJ. Bio-optical properties of the marine cyanobacteria
469 *Trichodesmium* spp. I. Absorption and photosynthetic spectra. Limnol. Oceanogr. 1999;
470 44: 608–617.

471 Suprasi KM, Kumar M, Segecova A, McCauley JI, Herdean A, Padula MP, O'Meara T, Ralph
472 PJ. Characterisation and bioactivity analysis of peridinin-chlorophyll *a*-protein (PCP)
473 isolated from *Symbiodinium tridacnidorum* CS-73. J. Mar. Sci. Eng. 2021; 9(12):1387.
474 https://doi.org/10.3390/jmse9121387

475 Suwa R, Hirose M, Hidaka M. Seasonal fluctuation in zooxanthellar genotype composition and
476 photophysiology in the corals *Pavona divaricata* and *P. decussata*. Mar. Ecol. Prog. Ser.
477 2008; 381:129-137.

478 Taheri P, Tarighi S. Riboflavin induces resistance in rice against *Rhizoctonia solani* via
479 jasmonate-mediated priming of phenylpropanoid pathway. J. Plant Physiol. 2010;
480 167:201–208. https://10.1016/j.jplph.2009.08.003

481 Venn AA, Wilson MA, Trapido-Rosenthal HG, Keely BJ, Douglas AE. The impact of coral
482 bleaching on the pigment profile of the symbiotic alga, *Symbiodinium*. Plant Cell
483 Environ. 2006; 29:2133-2142. https://doi.org/10.1111/j.1365-3040.2006.001587.x

484 Warner ME, Fitt WK, Schmidt GW. The effects of elevated temperature on the photosynthetic
485 efficiency of zooxanthellae *in hospite* from four different species of reef coral: a novel
486 approach. Plant Cell Environ. 1996; 19(3):291-299. https://doi.org/10.1111/j.1365-
487 3040.1996.tb00251.x

488 Wickham H. ggplot2: Elegant Graphics for Data Analysis. Springer New York. 2016.
489 https://doi.org/10.1007/978-0-387-98141-3

490 Yacobi YZ. From Tswett to identified flying objects: A concise history of chlorophyll *a* use for
491 quantification of phytoplankton. Isr. J. Plant Sci. 2012; 60(1).
492 https://doi.org/10.1560/IJPS.60.1-2.243

493 Yoon HS, Havkett JD, Bhattacharya D. A single origin of the peridinin- and fucoxanthin-
494 containing plastids in dinoflagellates through tertiary endosymbiosis. PNAS. 2002;
495 99(18):11724-11729.

496 Young A. Britton G. Carotenoids in Photosynthesis. Chapman and Hall, London, England. 1993.

497 Yu X, Liu H, Klejnot J, Lin C. The Cryptochrome Blue Light Receptors. Arabidopsis Book
498 2010; 8:e0135. https://doi.org/10.1199/tab.0135

499 Zapata M, Edvardsen B, Rodriguez F, Maestro MA, Garrido JL. Chlorophyll c_2
500 monogalactosyldiacylglyceride ester (chl c_2- MGDG). A novel marker pigment for
501 *Chrysochromulina* species (Haptophyta). Mar. Ecol. Prog. Ser. 2001; 219:85-98.
502 https://www.doi.org/10.3354/meps219085

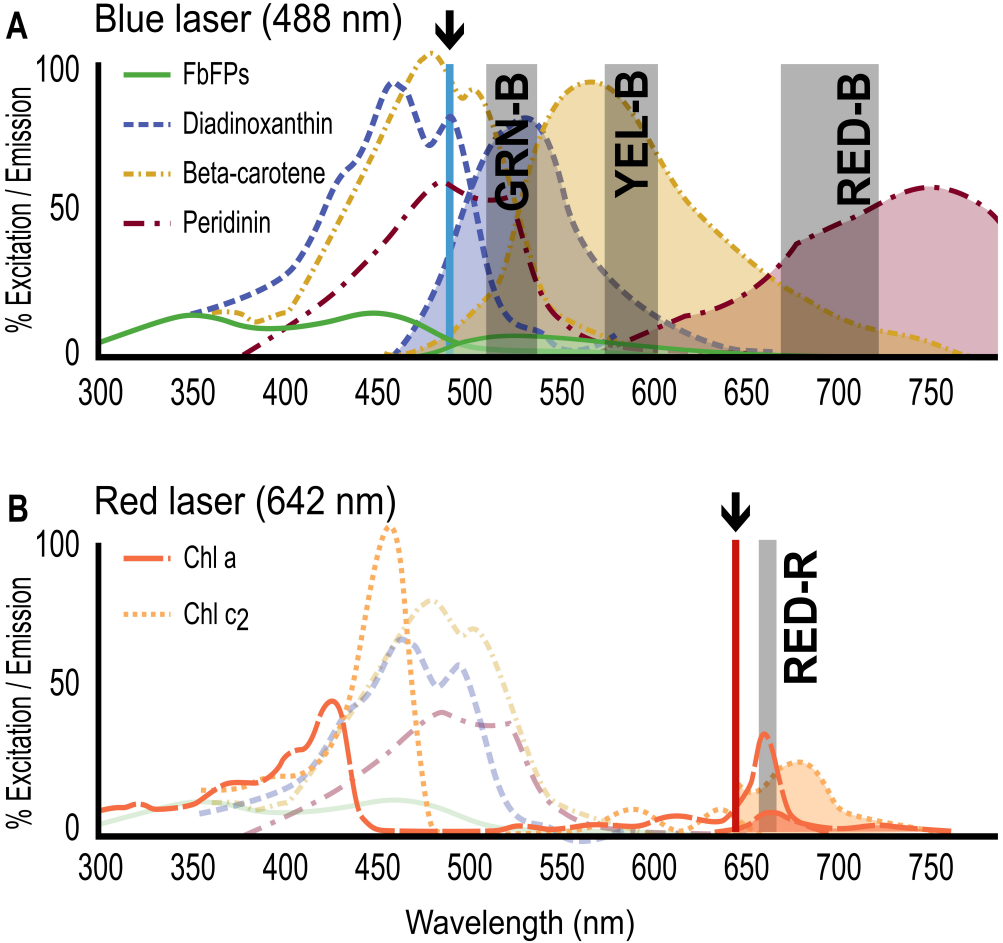
A
Blue laser (488 nm)
FbFPs
Diadinoxanthin
Beta-carotene
Peridinin
GRN-B
YEL-B
RED-B
% Excitation / Emission
100
50
0
300
350
400
450
500
550
600
650
700
750
B
Red laser (642 nm)
Chl a
Chl c2
RED-R
% Excitation / Emission
100
50
0
300
350
400
450
500
550
600
650
700
750
Wavelength (nm)

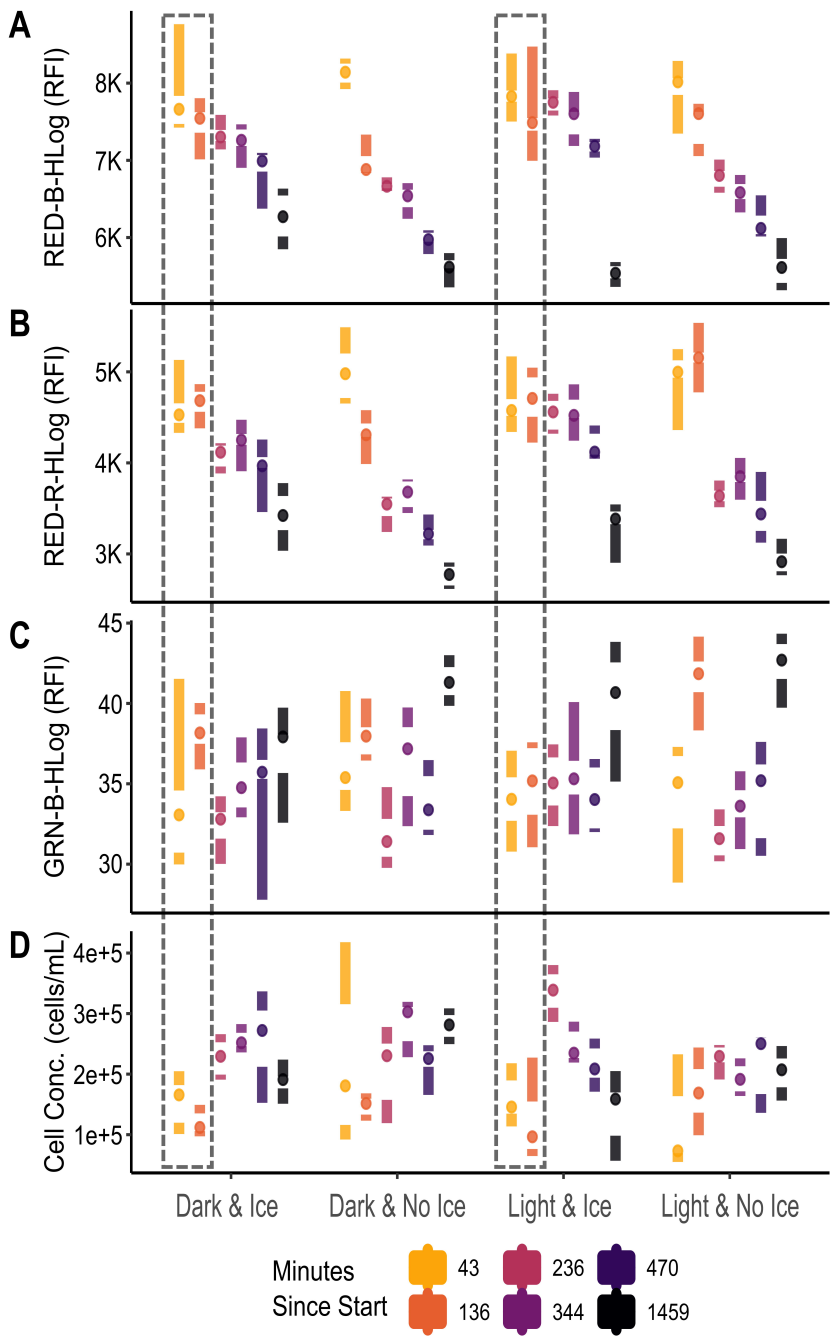
A
RED-B-HLog (RFI)
8K
7K
6K
B
RED-R-HLog (RFI)
5K
4K
3K
C
GRN-B-HLog (RFI)
45
40
35
30
D
Cell Conc. (cells/mL)
4e+5
3e+5
2e+5
1e+5
Dark & Ice
Dark & No Ice
Light & Ice
Light & No Ice
Minutes Since Start
43
136
236
344
470
1459

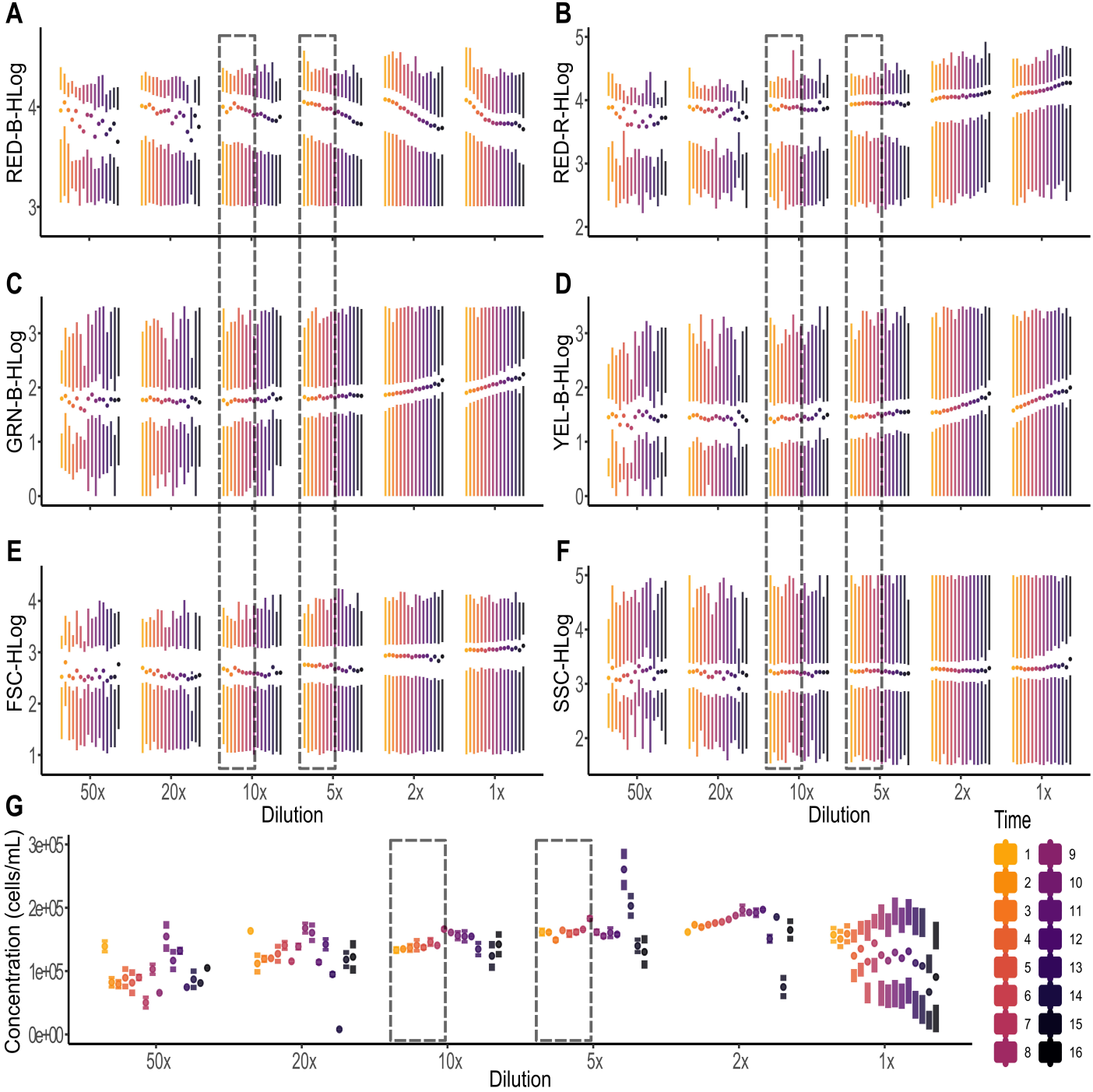
A
RED-B-HLog
B
RED-R-HLog
C
GRN-B-HLog
D
YEL-B-HLog
E
FSC-HLog
F
SSC-HLog
50x
20x
10x
5x
2x
1x
Dilution
G
Concentration (cells/mL)
3e+05
2e+05
1e+05
0e+00
Time
1
2
3
4
5
6
7
8
9
10
11
12
13
14
15
16

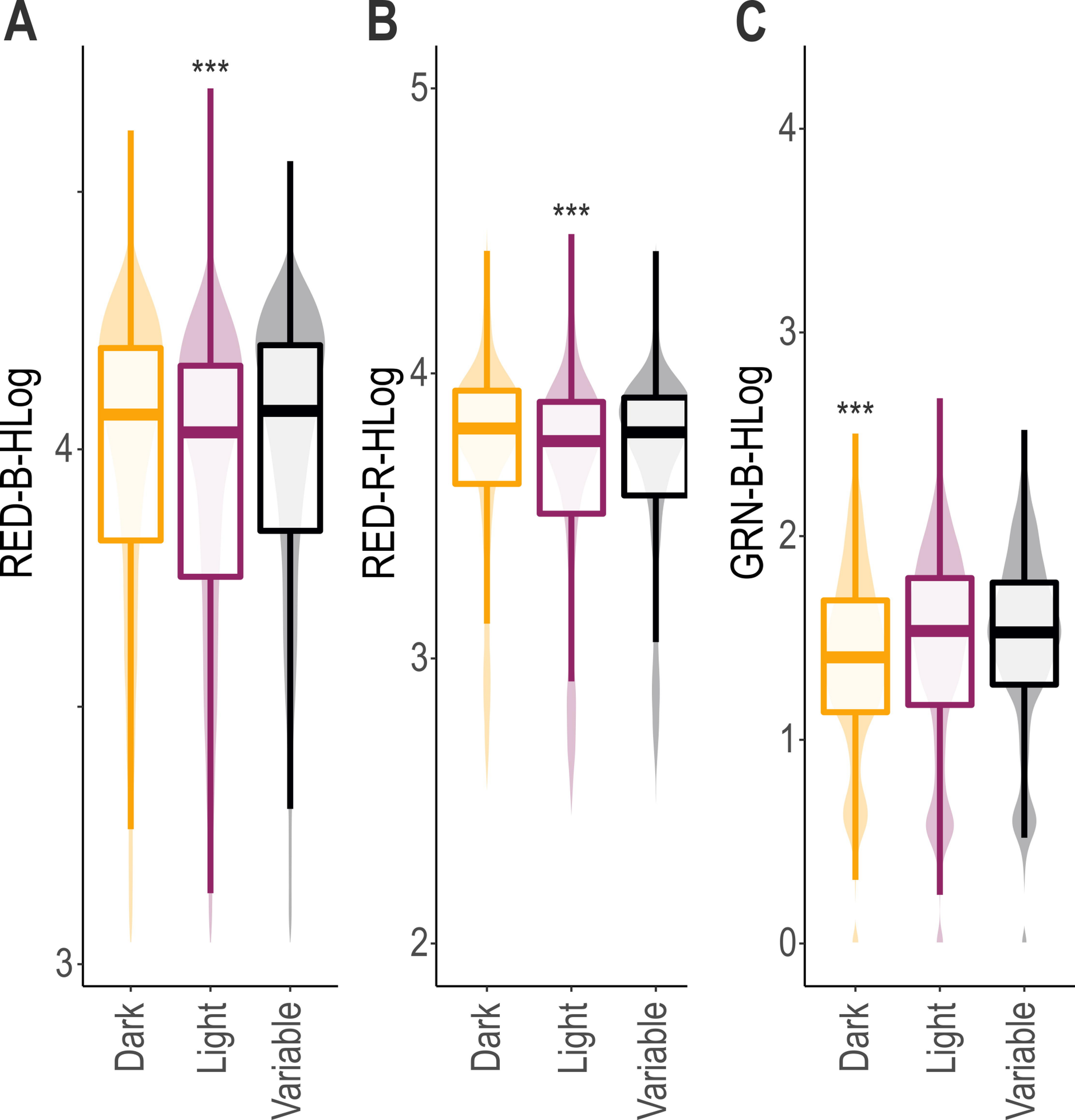
A
B
C
RED-B-HLog
RED-R-HLog
GRN-B-HLog
***
***
***
5
4
3
2
4
3
2
1
0
Dark
Light
Variable
Dark
Light
Variable
Dark
Light
Variable

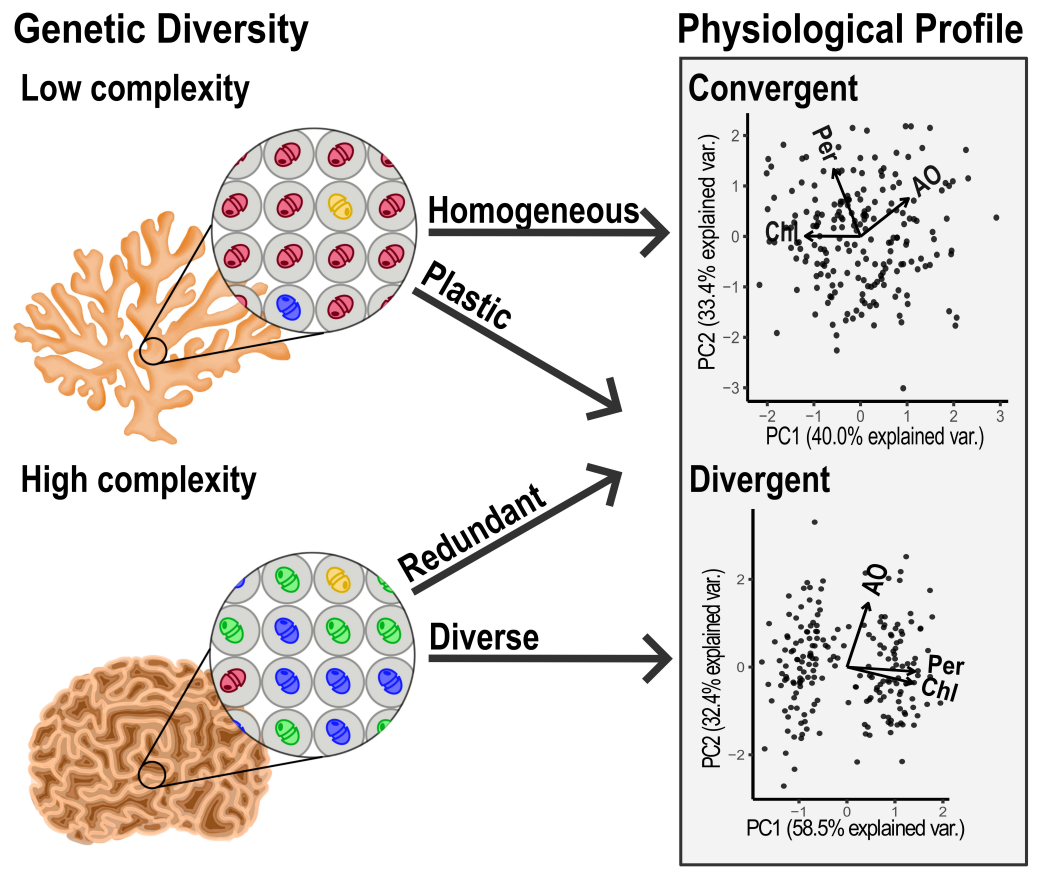
Genetic Diversity
Physiological Profile
Low complexity
Homogeneous
Plastic
Convergent
Per
AO
Chl
PC2 (33.4% explained var.)
PC1 (40.0% explained var.)
High complexity
Redundant
Diverse
Divergent
AO
Per
Chl
PC2 (32.4% explained var.)
PC1 (58.5% explained var.)